

THE UNIVERSE IN 3D

FIRST OBSERVATIONS WITH SPIFFI, THE INFRARED INTEGRAL FIELD SPECTROMETER FOR THE VLT

SPIFFI IS THE INFRARED INTEGRAL FIELD SPECTROMETER FOR THE VLT. HERE WE REPORT ON EARLY RESULTS FROM OUR FIRST OBSERVATIONS IN 2003. THIS SELECTION INCLUDES THE STELLAR CONTENT AND DYNAMICS OF THE GALACTIC CENTRE AND ITS GEOMETRIC DISTANCE MEASUREMENT, THE DYNAMICS AND MOLECULAR EMISSION OF THE ULTRA LUMINOUS INFRARED GALAXY NGC 6240, AND THE PORTRAIT OF THE HIGH-RED-SHIFT SUBMILLIMETER GALAXY SMM 14011+0252, INDICATING THAT SUBMILLIMETER GALAXIES ARE THE PRECURSORS OF MASSIVE LOCAL BULGES AND ELLIPTICALS.

F. EISENHAUER¹, M. TECZA¹,
N. THATTE^{1,2}, R. GENZEL^{1,3},
R. ABUTER¹, C. ISERLOHE¹,
J. SCHREIBER¹, S. HUBER¹,
C. RÖHRLE^{1,4}, M. HORROBIN¹,
A. SCHEGERER¹, A.J. BAKER¹,
R. BENDER^{1,5}, R. DAVIES¹,
M. LEHNERT¹, D. LUTZ¹,
N. NESVADBA¹, T. OTT¹,
S. SEITZ^{1,5}, R. SCHÖDEL¹,
L.J. TACCONI¹, H. BONNET⁴,
R. CASTILLO⁴, R. CONZELMANN⁴,
R. DONALDSON⁴, G. FINGER⁴,
G. GILLET⁴, N. HUBIN⁴,
M. KISSLER-PATIG⁴,
J.-L. LIZON⁴, G. MONNET⁴,
S. STRÖBELE⁴

¹Max-Planck-Institut für
extraterrestrische Physik, Garching,
Germany,

²Department of Astrophysics,
University of Oxford, U.K.,

³Department of Physics, University of
California, Berkeley, USA,

⁴European Southern Observatory,
Garching, Germany,

⁵Universitätssternwarte München,
Ludwig-Maximilians Universität,
Germany

SPIFFI (*SPECTROMETER FOR Infrared Faint Field Imaging*) is the new near-infrared field spectrometer for the VLT, developed at the Max-Planck-Institute for Extraterrestrial Physics (MPE, Eisenhauer et al. 2000). Here we report on the results of its first observing runs as a ‘guest instrument’ at the VLT in the February to April 2003 period. As of 2004 on, SPIFFI will be coupled to an adaptive optics module developed at ESO (Bonnet et al. 2003) to provide the SINFONI (SINGLE Faint Object Near-IR Investigation) facility. SPIFFI offers imaging spectroscopy of a contiguous, two-dimensional field of 32×32 spatial pixels in the 1.1 – 2.45 μm wavelength range and a resolving power of 1300–3500. As a result, the instrument delivers a simultaneous, three-dimensional data-cube with two spatial dimensions and one spectral dimension. SPIFFI is the successor to the MPE integral field spectrometer 3D, the world’s first infrared integral field spectrometer developed in the early 1990s.

When the new generation of 1024^2 pixels, near-infrared detectors became available in the mid-1990’s, we started the development of SPIFFI, for an order of magnitude increase in the number of spatial and spectral elements over 3D. Even more importantly, because of its fully cryogenic image slicer and high throughput optics, along with OH airglow suppression and smaller pixels, SPIFFI at the VLT delivers a factor of 20 to 50 improvement in point source sensitivity over 3D. This development attracted the attention of ESO, specifically because of its major advantages over long slit spectroscopy when operated together with adaptive optics. Simultaneous observation of a two-dimensional field is the best way to reach the full diffraction limited resolution in imaging spectroscopy, while

in addition minimizing slit losses. The development of such an adaptive optics assisted integral field spectrometer was subsequently recommended by the ESO Scientific and Technical Committee (STC) in 1997, and finally formalized in 2001 with a contract between ESO and MPE. Because the research and development program for SPIFFI had been launched long before the official start of the full project, we took advantage of this head start and brought SPIFFI to the VLT as a guest instrument for seeing limited observations, while integration of the adaptive optics module was starting at ESO-Garching.

THE INSTRUMENT: EVERY PHOTON, EVERY PIXEL

The primary goal of SPIFFI was to get a maximum number of spectra of a two-dimensional field in a single exposure, each spectrum covering a full near-infrared atmospheric wavelength band, J (1.1 – 1.4 μm), H (1.45 – 1.85 μm) or K (1.95 – 2.45 μm), with sufficiently high spectral resolution (~ 3000) to observe between the night sky emission lines. However, the format of infrared detectors is still rather limited when compared to optical CCDs, and the largest detector available at the start of the SPIFFI project had only 1024×1024 pixels. We thus decided to use every single detector pixel, simultaneously observing 32×32 (1024) spectra with 1024 spectral channels each. The second design criterion for SPIFFI was to provide small pixel scales (~ 25 mas) for diffraction limited observations, and in addition to allow seeing limited observations with as large as possible a field of view. In practice, the pixel size on the sky is limited by the minimum feasible f -number of the spectrometer camera. We finally pushed the camera design to a f -number of 1.45, so that SPIFFI can deliver a pixel

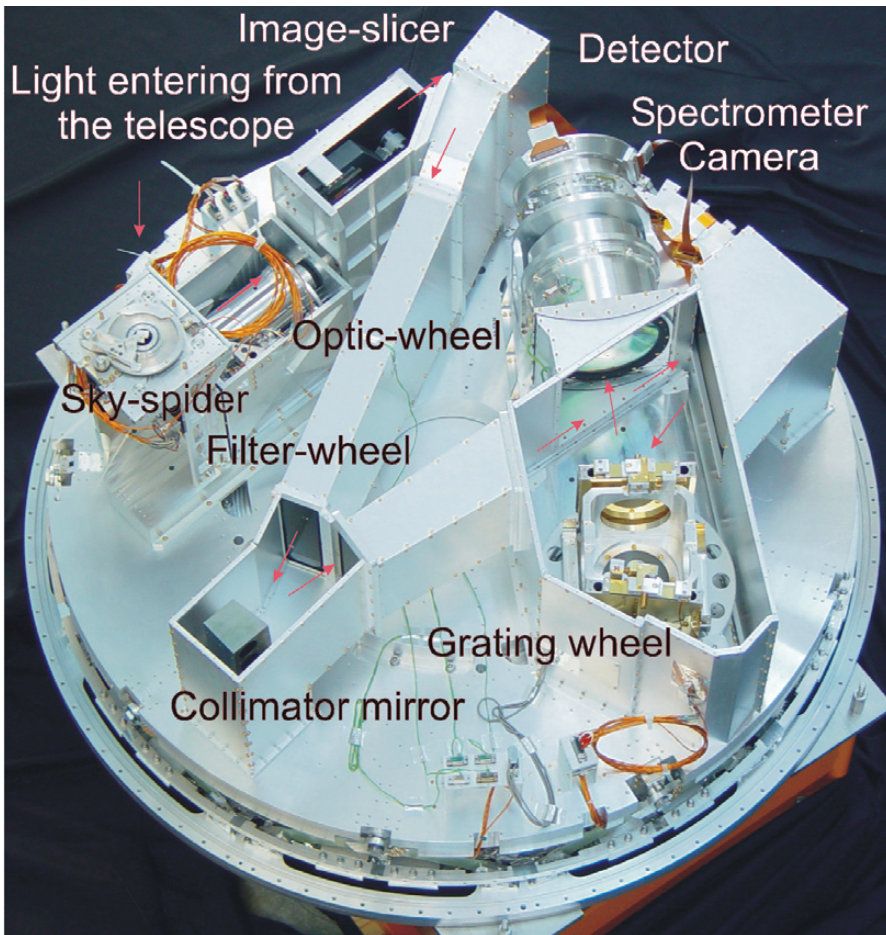


Figure 1: An inside view of SPIFFI: The light enters from the top, and passes the sky-spider. The pre-optics with a filter-wheel and interchangeable lenses provides three different image scales. The image slicer rearranges the two-dimensional field into a pseudo-long slit, which is perpendicular to the base plate. Three diamond turned mirrors collimate the light on one of the four gratings. A multiple-lens system then focuses the spectra on a Rockwell HAWAII array. The diameter of the instrument is 1.3 m.

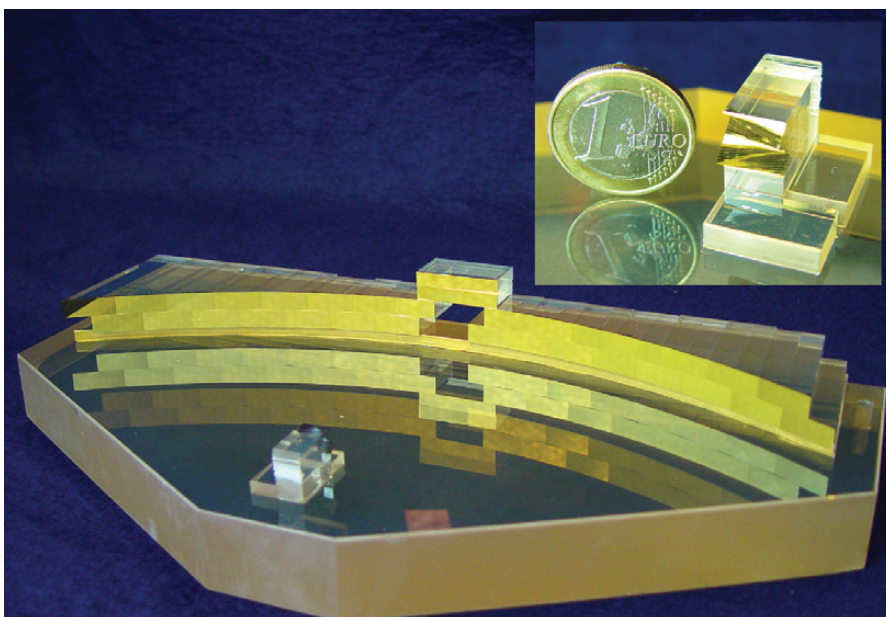


Figure 2: SPIFFI image slicer: The light enters through the hole in the big slicer. A stack of 32 small mirrors 'the' small' slicer – slices the image and redirects the light towards the 32 mirrors of the 'big' slicer, which rearranges the slitlets to a 31 cm long pseudo-long-slit. The small inset shows an enlargement of the small slicer.

size of 0.25", corresponding to a total field of view of 8" x 8". To make optimal use of the excellent seeing conditions in Paranal, and for partial correction of atmospheric turbulence with faint reference stars, SPIFFI also provides an intermediate image scale of 0.1"/pixel. In addition to spectroscopy of the J, H, and K-bands individually, the combined H and K bands (1.45 – 2.45 μm) can be observed at a lower spectral resolution.

Figure 1 shows the opto-mechanical components of SPIFFI. The entire instrument is cooled in a bath cryostat to the temperature of liquid nitrogen. Light enters SPIFFI from the top, and first passes the sky-spider. This device contains three motorized pairs of mirrors, which reflect the light from an off axis sky field up to 45" away from the object onto the image slicer field of view for simultaneous measurement of the sky background. Below the sky-spider, a motorized pre-optics provides three different image scales, the filters, and a cold stop for the suppression of the thermal background. The focus of the pre-optics is located at the 'small slicer' (Figure 2). This part of the image slicer consists of a stack of 32 plane mirrors, which slices the image into slitlets sent in different directions. A second set of 32 mirrors, the 'big slicer', collects the light and forms a pseudo-long-slit (Fig.2). To avoid differential thermal contraction, the unit is made completely from zero expansion glass. All parts (approximately 70 in number) are optically contacted.

After the image has been sliced and re-arranged to the pseudo slit, three diamond turned mirrors collimate the light onto the gratings. The gratings are directly ruled in gold on an aluminium substrate and blazed to the centre of their bandpass for optimum efficiency. The spectrometer camera is a six-lens system with an aperture of 160 mm. When operated at adaptive optics pixel scales, the demands on the instrument flexure are very stringent. We have thus implemented an inductive metrology system, which measures the relative motion of the cold structure with respect to the cryostat lid, and provides the input for the secondary guiding.

COMMISSIONING: NEVER WASTE A MINUTE OF TELESCOPE TIME

After its final tests at the VLT Cassegrain focus simulator in Garching in December 2002, the instrument arrived on Paranal on 9 January, 2003. After one week of integration, the SPIFFI team (Fig.3) cooled down the instrument successfully. On 6 February 2003, SPIFFI was transported to the VLT observatory platform.

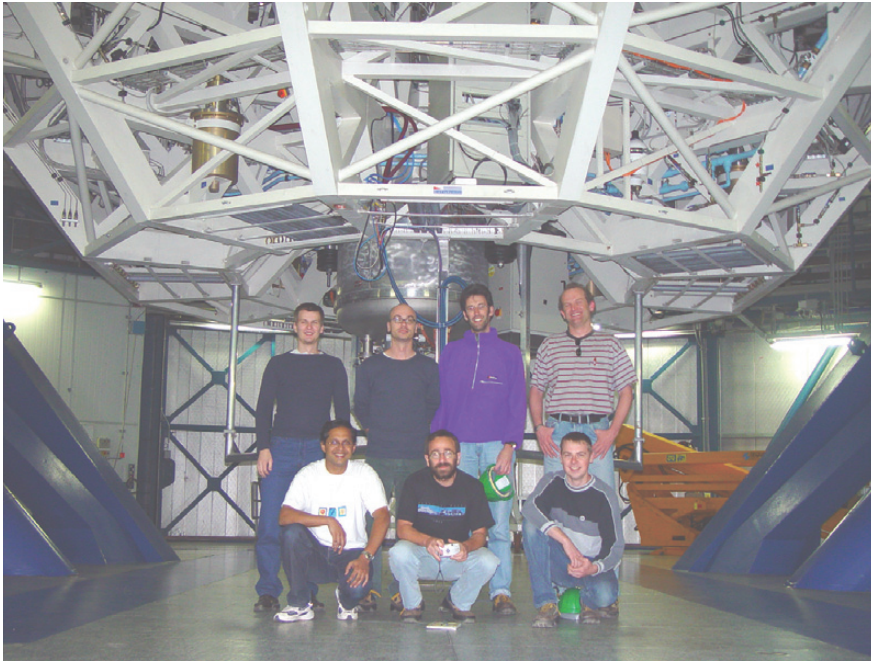


Figure 3: SPIFFI at the telescope: The picture shows members of the SPIFFI team after the successful installation of the instrument at the Cassegrain focus of Kueyen: From left to right: C. Iserlohe, N. Thatte, J. Schreiber, R. Abuter, F. Eisenhauer, S. Huber, M. Tecza. Not shown but present during commissioning or observing: R. Genzel, M. Horrobin, C. Röhrle, D. Lutz, A. Schegerer.

During the nights from February 8 through 13, SPIFFI was commissioned. Thanks to careful definition and verification of the telescope-instrument interface, the first target HD23561 immediately appeared within a few arcseconds of the SPIFFI field centre. The best images taken with the $0.1''/\text{pixel}$ scale during science operation in March and April had a FWHM of approximately $0.25''$ in K-band. More than 30% of all photons in H- and K-Band arriving at the telescope are eventually detected. The total efficiency in J-Band is approximately 20%. The average optical transmission of SPIFFI including pre-optics, filter, image-slicer, spectrometer-optics, and grating is approximately 37%, 47%, and 42%, for the J-, H-, and K-band, respectively. With this overall transmission, SPIFFI significantly outperforms competing integral field spectrometers. The spectral resolving power as measured on night-sky emission-lines is approximately 3500 in K-Band, 2500 in H-Band, 2000 in J-Band and 1300 in the combined H&K band.

SPIFFI's operation is straightforward, and requires no in-depth knowledge of integral field spectroscopy. A quick-look image reconstruction allows the instantaneous display of the reconstructed image during acquisition and observing. The normal mode of observing is nodding between the science field and blank sky, which allows accurate subtraction of the night sky emission and the thermal emission of the telescope. Alternatively, SPIFFI was operated in a 'stare'-mode, in which no separate sky-field is observed, but in which the night-sky contribution to

the source spectrum is subtracted from a measurement within the instrument field of view. For a small object, which fills only part of the SPIFFI field of view, the night-sky spectrum can be extracted directly from its surroundings. Larger objects, which fill the whole SPIFFI field of view, are observed with the sky-spider. While this stare-mode doubles the on-source observing time, the quality of the sky-subtraction is limited by the accuracy of the instrument calibration, specifically the flat field, and detector instabilities. In practice, the noise in the stare-mode observations is presently a factor of a few above the photon noise. We are currently investigating improved data-reduction techniques based on a Bezier-Spline representation of the night-sky emission to optimally recover the sky-free spectrum of the object of interest.

Because of the various peculiarities of the raw data from integral field spectroscopy SPIFFI has its own data reduction software. This package provides all tools for the calibration and reduction of SPIFFI data, including wavelength calibration and image reconstruction. The final data format is a three-dimensional data cube with 32×32 spatial pixels, and up to 2560 spectral elements.

FIRST RESULTS

In the following we will discuss some of the scientific results obtained during the guest instrument runs in March and April 2003. To give the readers a feel for the kind of science that can be obtained with an integral field instrument we present here three highlights in different areas

– our own Galactic Centre, a $z=0.024$ infrared luminous merger and a $z=2.5$ submillimeter galaxy - rather than making a broad sweep of all the observations that were carried out during the 15 observing nights. These results are also discussed in greater detail in several papers that are submitted/in press (e.g. Genzel et al. 2003b, Eisenhauer et al. 2003).

STELLAR POPULATIONS AND DYNAMICS OF THE GALACTIC CENTRE STAR CLUSTER

The Centre of the Milky Way is a unique laboratory for studying physical processes that are thought to occur generally in galactic nuclei (see Ott et al. 2003). High resolution, near-IR integral field spectroscopy offers a unique opportunity for exploring in detail the properties, dynamics and evolution of the nuclear star cluster in the immediate vicinity of a supermassive black hole. We observed the central parsec region with SPIFFI during two nights (for about an hour each) and created two mosaics of the central region, one covering the central parsec with $0.25''$ pixel resolution (FWHM $\sim 0.75''$) at $R \sim 1300$ in the combined H&K mode, and one of the central $\sim 6''$ with $0.1''$ pixels at $R \sim 3500$ in K (Fig. 4). In the latter case, the effective spatial resolution was a remarkable $0.27''$ FWHM, providing us with the by far deepest (K $\sim 15-16$) and highest resolution imaging spectroscopy data set obtained up to this time.

With this new data set, it is possible to probe in more detail the stellar composition of the central parsec. We found about 40 massive early type stars in the region mapped, mostly from stellar emission lines, thereby almost doubling the number of spectroscopically identified early type stars (mostly of type WN9-10, Ofpe or luminous blue variables LBVs). Our new data also clearly detect, for the first time, an early, hot WN star (WN5/6: $T_{\text{eff}} \sim 40-45$ kK, Figure 5), as well as a large number of WC stars (Fig. 4, 5). The ratio of WC to WN stars is about 1, and the ra-

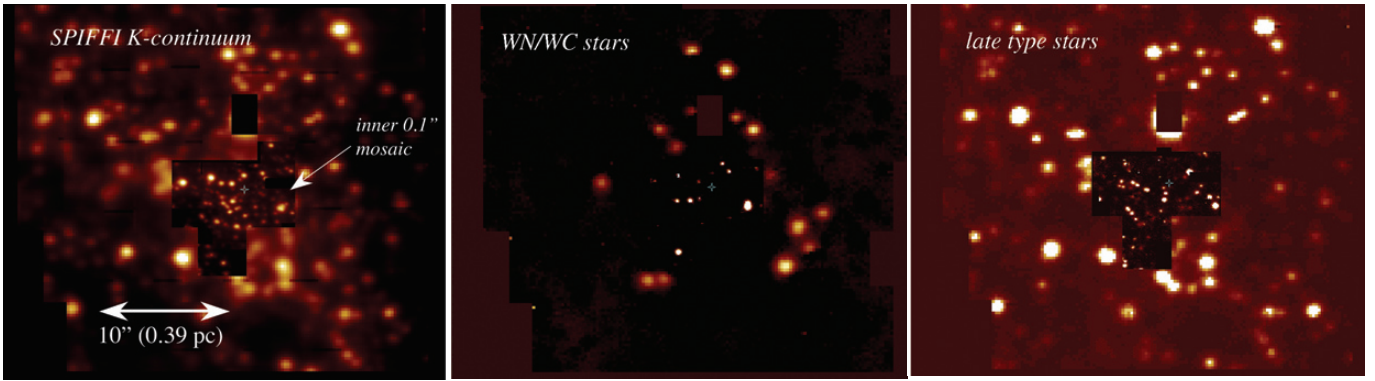


Figure 4: SPIFFI continuum and line images of the Galactic Centre. The light blue asterisk marks the position of the supermassive black hole/SgrA*. Left: K-band image constructed from an outer mosaic of 0.25'' pixel data cubes (~0.75'' resolution), as well as an inner mosaic of the central ~10'' at a pixel scale of 0.1'' and FWHM 0.27''. Middle: continuum subtracted line image near Hel 2.113mm, marking the positions of the Wolf-Rayet (WN, WC) stars. Right: continuum subtracted CO 0-2 absorption line flux, marking the positions of late type stars.

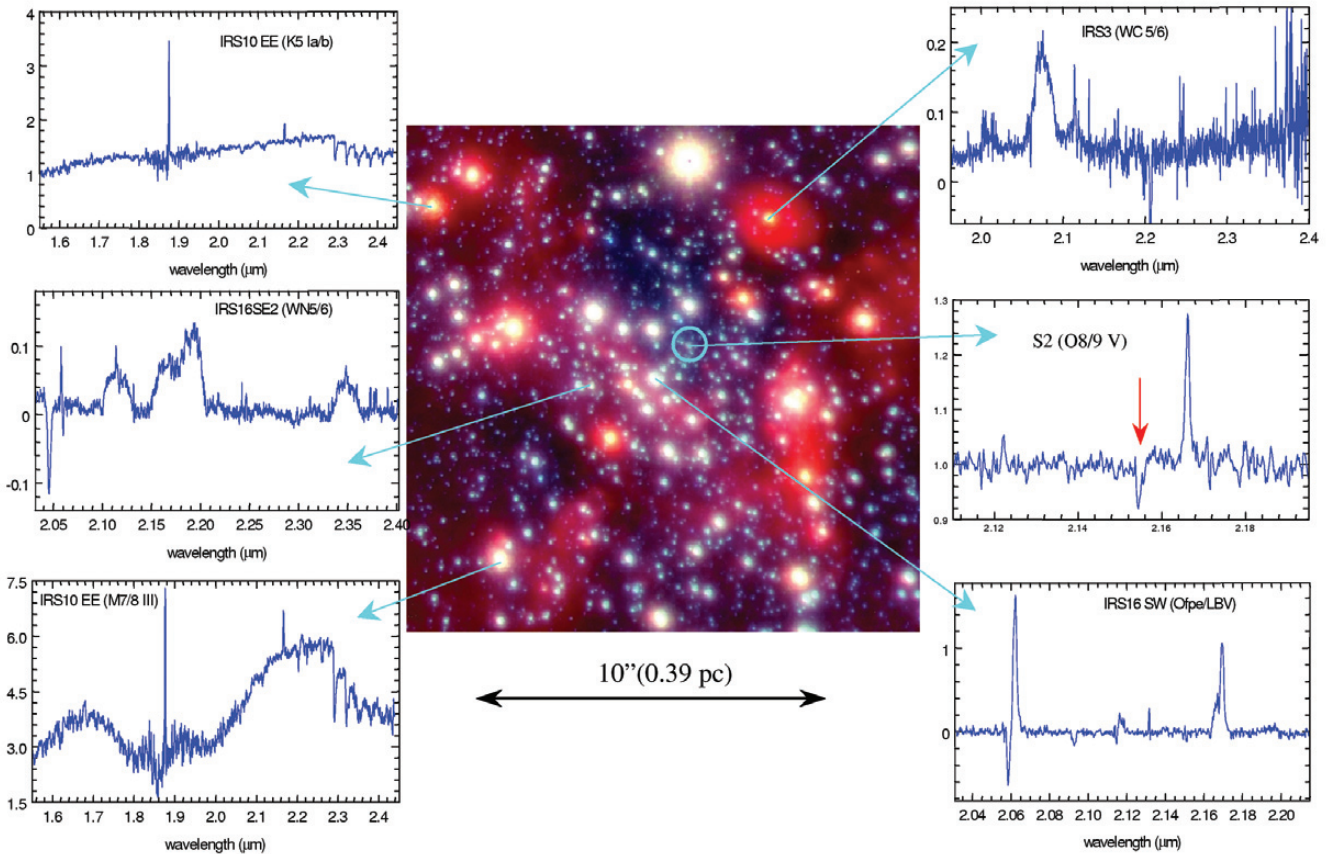


Figure 5: Selected SPIFFI spectra superposed on a NACO H/K/L' colour composite image of the central region. The spectra display the wide range of stellar types found in the cluster, ranging from late type main sequence O stars (the star S2 near SgrA*, oval in image), to luminous blue variables (IRS16SW, lower right), early WN (middle left) and WC (top right) Wolf-Rayet stars, to red supergiants (the brightest star IRS7 at the top/middle of the image), bright asymptotic giant branch stars (IRS9, lower left) and normal red giants (top left). Note that in the case of the dusty WC5/6 star IRS 3 (top right) we first subtracted a strong featureless power-law to emphasize the characteristic carbon-features.

ratio of (narrow-line) LBVs, such as IRS16C, NW and SW, to WN stars is about 0.5. Despite the much superior high resolution, inner cube (much less susceptible to veiling of stellar Br γ absorption by the diffuse Br γ emission from the SgrA West HII region), there is (still) no evidence for main sequence O-stars, with the exception of the innermost arcsecond. The WR/O star ratio in the nuclear star cluster thus appears to be greater than

about 20. Several of the mid-IR excess stars in the central region (very red color in Fig. 5), including the brightest 10 μ m source in the central parsec, IRS 3, are WC stars. As a WCE (WC5/6) star IRS3 may be a prime candidate for exploding as a supernova in the next few 10⁴ years. Other such dusty sources can now be shown from their spatial distribution and proper motions to be luminous early type stars that happen to move into and

strongly heat the dust in the HII region (Genzel et al. 2003b).

The unique simultaneous H&K capability allows to unambiguously distinguish moderately late type (K2-5) supergiants from AGB stars. Both types have equivalent near-IR flux densities. The much later type (M4-9 III) AGB stars, however, exhibit deep water vapour, steam troughs between the H and K-bands that can be easily recognized in our

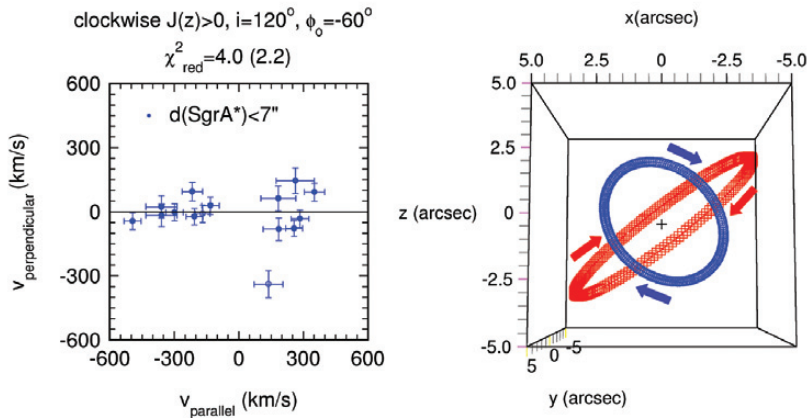


Figure 6: Dynamical properties of early type stars in the Galactic Centre. Left: projection of 3D space velocities of clockwise (on the sky) rotating stars, perpendicular to the best fitting plane, at inclination 120° with respect to the sky, and -60° of the line of nodes, east of north. 14 of the 15 stars with three space velocities adhere to rotation in a fairly thin plane in this orientation. Likewise most of the counter-clockwise stars largely also follow a disc rotation pattern. Right: Orientation of the two young star discs. East-west on the sky is left-right, and the line of sight direction is up-down (the observer sits at $z=-\infty$). The two discs counter-rotate with respect to each other, but both exhibit rotation that is counter to Galactic rotation.

data (source IRS9 in the lower left inset of Fig. 5). This finally settles a long debate about the properties of the brightest late type stars in the central parsec: of the dozen or so $K < 10.5$ late type stars ($M(K) < -7.2$), a maximum of two are supergiants, the rest are clearly AGB stars.

The large ratio of Wolf-Rayet stars to O-stars, the large WC/WN ratio, and the large blue to red supergiant ratio, in comparison with recent star cluster models, indicate that the young stars in the Galactic Centre originated in a high metallicity starburst about 5 Myr ago. The unusually large number of luminous LBV stars, most of them in the central IRS16 cluster, suggests that this burst had a duration of several Myr and that the massive stars may be fast rotators, thereby allowing the presence of very massive ($\geq 100 M_\odot$) stars near the Humphreys-Davidson limit of stability.

The combination of proper motions and radial velocities of the massive stars allows a detailed analysis of their dynamical

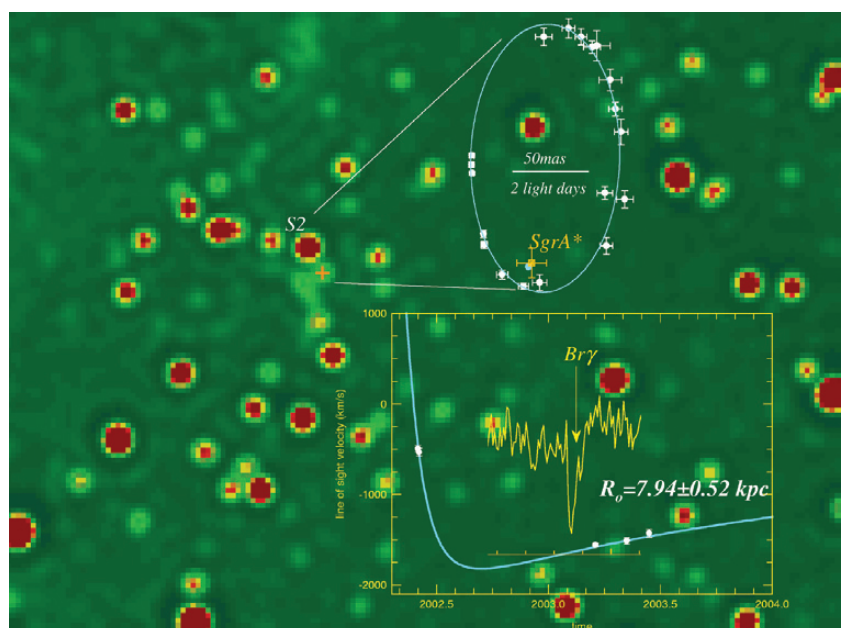
properties. The surprising result (Genzel et al. 2003b) is that essentially all young stars in the central $10''$ belong to one of two well defined, rotating stellar rings/discs. The two young star discs are at fairly large angles with respect to each other but share a common, counter-Galactic rotation (Fig. 6). Combined with the fact (see above) that both discs have essentially the same stellar content these data offer valuable constraints on one of the most perplexing current riddles in Galactic Centre research: how can the central $0.1-10''$ host so many young, massive stars? The environment and the presence of strong tidal forces from the black hole make star formation from cloud col-

lapse extremely difficult, if not impossible, and mass segregation of the massive stars from further out is excluded because of their short lifetimes. The presence of two, coeval stellar discs suggests that a highly dissipative and sudden event was at play in the formation of the massive stars. One possibility is the collision of two infalling clouds, followed by the settling of the remaining debris into two separate discs orbiting the central black hole, and subsequent star formation.

A GEOMETRIC DETERMINATION OF THE DISTANCE TO THE GALACTIC CENTRE

The distance between the Sun and the Galactic Centre (R_\odot) is a fundamental parameter for determining the structure of the Milky Way. Through its impact on the calibration of the basic parameters of standard candles, such as RR Lyrae stars, Cepheids and giants the Galactic Centre distance also holds an important role in establishing the extragalactic distance scale. Ten years ago Reid (1993) summarized the state of our knowledge on R_\odot . At that time the only primary (geometric) distance indicator to the Galactic Centre came from the “expanding cluster parallax” method” applied to two H_2O masers in SgrB2, resulting in values of 7.1 and 6.5 kpc for the distances, with a combined statistical and systematic (1σ) uncertainty of ± 1.5 kpc. In addition there was a number of secondary (standard candle) determinations, based on RR-Lyrae stars, Cepheids, globular clusters and giants, as well some tertiary indicators, derived from theoretical constraints (e.g. Eddington luminosity of X-ray sources, Galaxy structure models). Since then Hipparcos data have improved the uncertainties of

Figure 7: Geometric determination of the Sun-Galactic Centre distance R_\odot from a precision measurement of the orbital parameters of the star S2 that is orbiting the central supermassive black hole. The star's line-of-sight motion is measured via the Doppler shift of the $Br\gamma$ line in terms of an absolute velocity (SPIFFI data as well as spectroscopic data from NIRSPEC (Keck, Ghez et al. (2003) and from NACO), whereas its proper motion is measured in terms of an angular velocity (data from SHARP/INTT and NACO). The orbital solution ties the angular and absolute velocities, thereby yielding the distance to the S2/SgrA* binary system.



the secondary determinations. The best present value of R_0 is ~ 8 kpc, with a combined statistical and systematic uncertainty of ± 0.5 to ± 1 kpc.

The SPIFFI observations allowed us to derive a primary distance measurement to the Galactic Centre with an uncertainty of only 5%. This determination has become possible through the advent of precision measurements of proper motions and line-of-sight velocities of the star S2. This star is orbiting the massive black hole and compact radio source SgrA*, and the classical ‘orbiting binary’ technique can then be applied to obtain an accurate determination of R_0 that is essentially free of systematic uncertainties in the astrophysical modelling. The essence of the method is that the star’s line-of-sight motion is measured via the Doppler shift of its spectral features in terms of an absolute velocity, whereas its proper motion is measured in terms of an angular velocity. The orbital solution ties the angular and absolute velocities, thereby yielding the distance to the binary. For the analysis of our measurements, we fitted

the positional and line-of-sight velocity data to a Kepler orbit, including the Galactic Centre distance as an additional fit parameter. Taking the first two radial velocity data of S2 obtained by Ghez et al. (2003), the SPIFFI data, the two NACO spectroscopy points, and the 19 positions from SHARP and NACO, our measurements deliver 43 data points to robustly fit 9 parameters of the S2 orbit as well as the Galactic Centre distance, resulting in $R_0 = 7.94 \pm 0.42$ kpc (Eisenhauer et al. 2003). This result confirms and significantly improves the earlier primary distance measurements and gives confidence in the quality and robustness of the standard candle methods that are at the key of the second rung of the extragalactic distance ladder.

A GALACTIC SHOCK IN THE MERGER NGC6240

The infrared luminous galaxy NGC6240 ($D=97$ Mpc, $L_{\text{IR}} = 6 \cdot 10^{11} L_{\odot}$) is in many ways a prototype for the class of gas rich, infrared (ultra-) luminous mergers that dominate the upper end of the local lumi-

nosity function of IRAS galaxies. The NGC6240 system has two rapidly rotating, massive bulges/nuclei at a projected separation of $1.6''$ (750 pc, upper left inset in Fig. 8), each of which contains a powerful starburst and a luminous, highly absorbed, X-ray active AGN (Tecza et al. 2000, Komossa et al. 2003, Lutz et al. 2003). As such, NGC6240 is probably a local template for the population of dust and gas rich, merger/AGN systems at high redshift that likely contribute about half of the energy density at $z \sim 2.5$ (see the section on SMMJ14011+0252). About $2 \cdot 10^9 L_{\odot}$, or 0.3% of the infrared luminosity emerges in H₂ infrared line emission, and the origin and excitation of this spectacular line emission has been subject of many studies. The K-band spectrum is full of vibrationally excited H₂ lines with excitation potentials up to about 20,000 K above the ground state (right inset, Fig. 9).

We observed NGC6240 with SPIFFI in K-band in excellent seeing ($0.27''$ FWHM) with the $0.1''/\text{pixel}$ scale. Figure 8 compares the distribution of the stellar light with that of the ionized gas (bottom

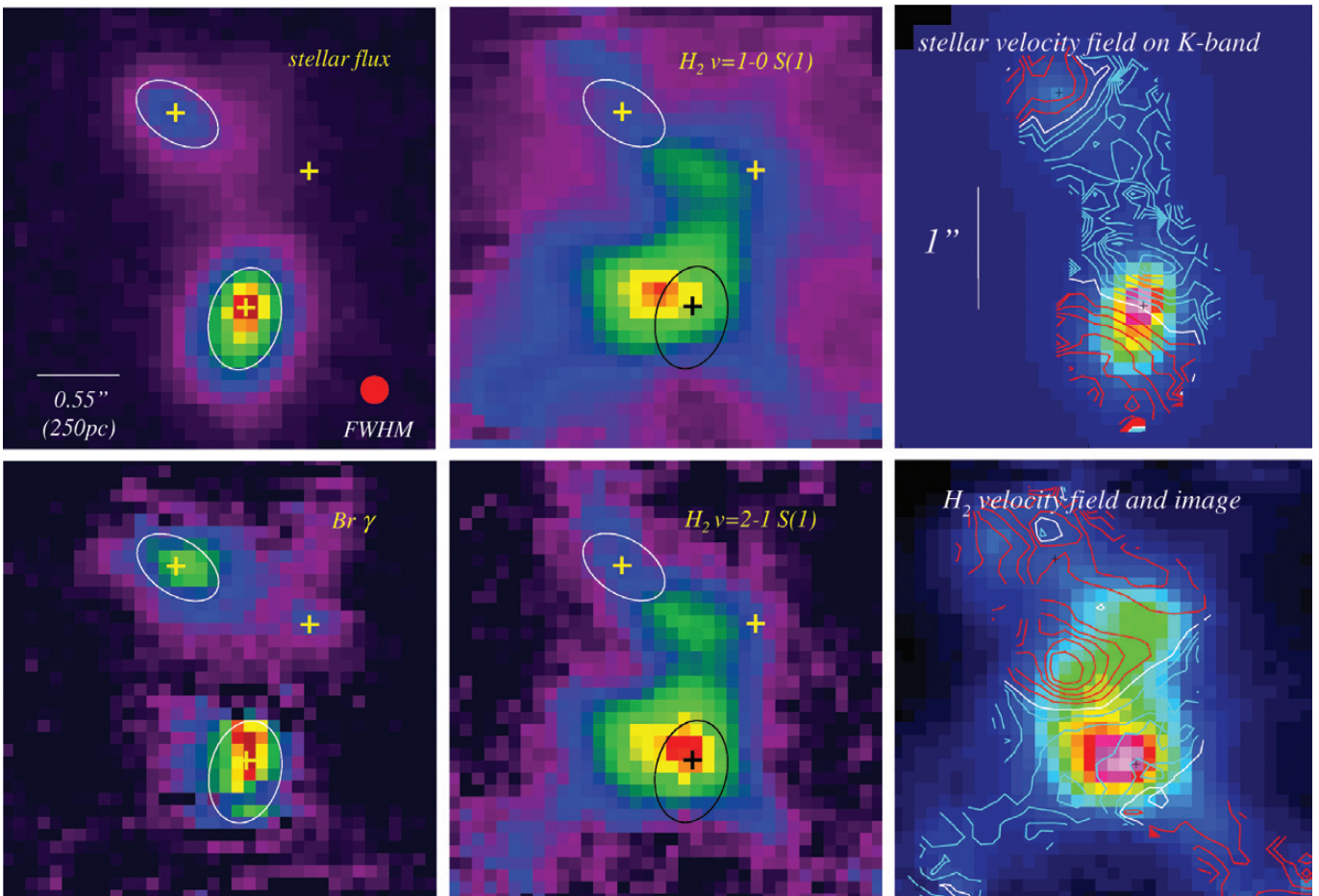


Figure 8: SPIFFI images, stellar and H₂ kinematics of the infrared luminous merger NGC6240. Stellar light (upper left, from CO 0-2 absorption flux), Br γ flux (bottom left), H₂ $v=1-0$ S(1) and $v=2-1$ S(1) flux distributions (middle insets). In all images the position of the two nuclei and their outer contours and of an extra-nuclear Br γ source are marked. Top right: stellar velocity field (contours) superposed on K-band image. The contour lines are in steps of 50 km/s, red and blue of the systemic velocity at 7300 km/s (white line). Bottom right: H₂ $v=1-0$ S(1) velocity contours (same units as for stars) on H₂ image.

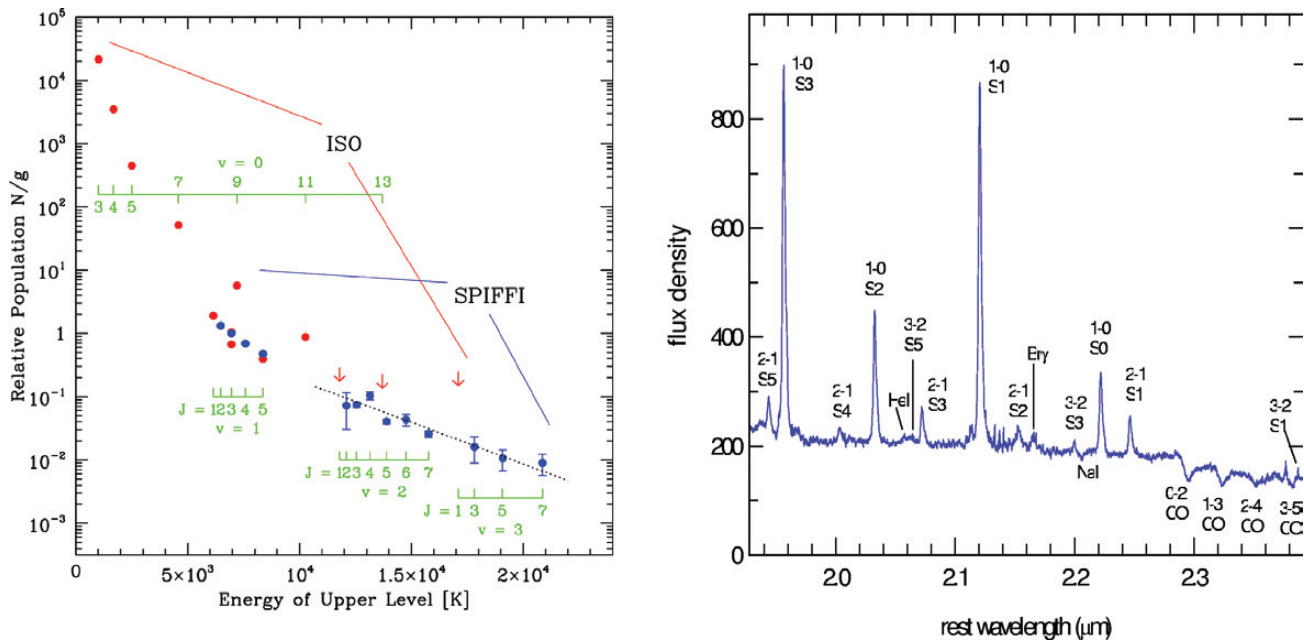


Figure 9: K-band spectrum (right, $0.5''$ aperture near southern nucleus) and level diagram (left) of H_2 rotationally excited and ro-vibrationally excited states (blue: SPIFFI, red: ISO SWS, Lutz et al. 2003). A constant temperature distribution is a straight line in this diagram, with a slope inversely proportional to temperature. The NGC6240 data indicate the presence of a wide range of excitation temperatures up to about 3300K (dotted black line fitting the $v=2$ and $v=3$ data). The offset between $v=0$ and $v>0$ data may either be due to extinction, or due to an additional component of somewhat cooler material. The distribution can be fit by a combination of J- and C-shock models, or by a bow-shock model.

left) and vibrationally excited molecular hydrogen (middle insets). Most of the starburst activity (as traced by Br γ) occurs in the two nuclei on scales of 200 pc, although there appears to be one extranuclear Br γ source in the gas bridge between the two nuclei, suggestive of star formation there. The vibrationally excited H_2 is very different and follows a complex spatial and dynamical pattern (lower right inset of Fig. 8) with several extended streamers. The high-resolution SPIFFI data now permit us to follow the H_2 distribution, excitation and kinematics on $\leq 10^2$ pc scales. The two middle insets show that $v=2-1$ and $v=1-0$ emission lines exhibit very similar large-scale distributions. The only difference occurs in the most prominent H_2 peak, where the higher excitation $v=2-1$ S(1) line is located closer to but still off the southern nucleus. The H_2 kinematics is extremely complex (lower right inset in Fig. 8) and very different from the relatively simple counter-rotation pattern of the stars (top right, Fig. 8).

The gas bridging the two nuclei is redshifted relative to the northern and southern nucleus and exhibits a very steep velocity gradient of 500 km/s over $0.7''$ as it curves around toward the southern nucleus. There it appears to ‘crash’ into the nuclear regions approximately at right angles relative to the stellar rotation pattern and with a velocity of 150 to 200 km/s relative to the stars. From the bright H_2 peak just NE of the southern nucleus two gas streamers emerge and envelop the southern galaxy. This kinematic pattern resembles the gas bridges found in simulations of gas rich mergers after the first peri-approach. We may be observing the two galaxies after the first ‘hang out’ phase in the process of falling back in for the second peri-approach. In the process, they are strongly interacting with and shock exciting the tidally swept out gas bridge between the nuclei.

Figure 9 shows an excitation diagram of the H_2 emission, where we have combined the SPIFFI data with ISO SWS measurements of the rotational line emission (Lutz et al. 2003). The H_2 level populations follow a smooth distribution with local excitation temperature steadily increasing with level energy (the slope of the local level distribution is inversely proportional to excitation temperature). The highest excitation lines we observe require an excitation temperature of about 3300 K. With the possible exception of the region very near the southern nucleus, the H_2 spatial distribution, kinematics and level populations thus strongly favor a ‘galactic shock’ model as the origin of the spectacular H_2 emission. The high temperature and turbulence also explains why little star formation as of yet

has occurred in the dense molecular gas bridge between the two nuclei. The cooling time of that gas is $\leq 10^7$ years, comparable to the time to the second peri-approach of the two nuclei. At this point NGC6240 will probably experience an even stronger star formation episode that will turn the system into a true ‘ultra’-luminous galaxy.

PORTRAIT OF A $z=2.5$ SUBMILLIMETER GALAXY

The strength of the extragalactic mid- and far-IR/submillimeter background indicates that about half of the cosmic energy density (excluding the microwave background) comes from distant, dusty starbursts and AGN. Surveys with ISOCAM at 15 μm , SCUBA at 850 μm , and MAMBO at 1200 μm suggest that this background is dominated by luminous and ultra-luminous infrared galaxies (LIRGs/ULIRGs: $L_{\text{IR}} \sim 10^{11.5-13} L_{\odot}$) at $z \geq 1$ (e.g. Genzel & Cesarsky 2000). Little is known yet about the physical properties of this important ‘submillimeter’ galaxy population since they are very faint in the rest wavelength UV/visible range. Half a dozen SCUBA sources presently have mm-confirmed spectroscopic redshifts near $z \sim 2.5$ (e.g. Genzel et al. 2003b, Downes & Solomon 2003), close to the redshift of the peak of cosmic star formation and QSO activity. The submillimeter population may trace the formation of massive/luminous AGN/starburst systems that may evolve into massive local early type and bulge galaxies.

One of the brightest SCUBA galaxies is the source SMMJ14011+0252 at $z=2.565$, which is gravitationally lensed by the foreground $z=0.25$ cluster Abell 1835

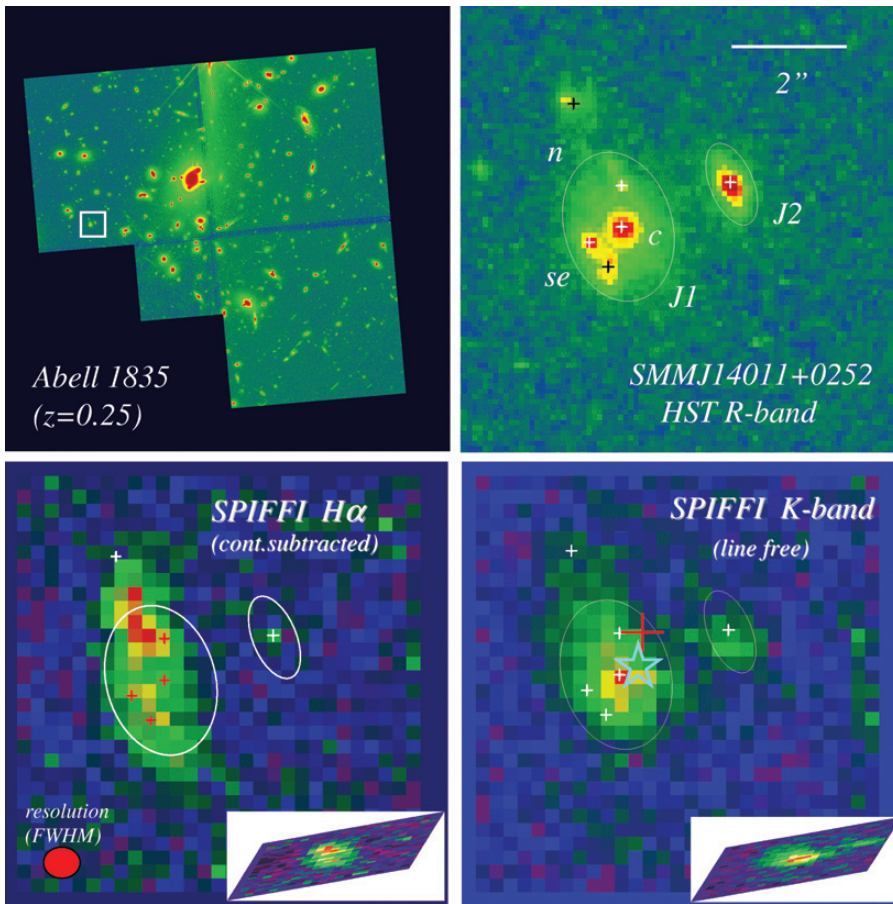


Figure 10: The SCUBA galaxy SMMJ14011+0252 ($z=2.565$). Top left: R-band HST WFPC2 image of the $z=0.25$ cluster Abell 1835, which gravitationally lenses the background submm galaxy SMMJ14011+0252 by about a factor of 4 to 6. Top right: HST R-band image of the central few arcseconds of the source with a log-scale color stretch (white square in left inset, from Ivison, priv. comm.). Bottom right: Line free K-band continuum image obtained with SPIFFI. The red cross is the position of the 1.4GHz radio emission (Ivison et al. 2001), and the blue asterisk marks the position of the CO mm line and continuum emission (Downes & Solomon 2003). Bottom left: Continuum subtracted SPIFFI $H\alpha$ map. At the bottom right of the lower insets we show the morphologies of the $H\alpha$ and K-band maps when correcting for a lensing magnification of 5 along p.a. 10° .

(Fig. 8, Ivison et al. 2001). HST imaging shows that the system consists of several sub-components (J1 (c, se, n), J2) spread over about $3''$ (Fig.10, 24 kpc without correction for lensing). We observed SMMJ14011 with SPIFFI in J, H and K-bands at the $0.25''$ pixel scale for a total of 15 hours on-source integration. The effective resolution in the different data sets is between 0.5 and $0.75''$. The lower right inset of Fig. 10 shows the line free K-band continuum distribution. In comparison to the HST image (Ivison et al. 2001, appropriately smoothed to the same resolution as the SPIFFI data), the rest-frame optical (\sim R-band) distribution is dominated by the extended J1 complex (white oval in Fig. 8), with a significant extension to the NNE. The blue knots J2 and J1se are not as prominent in the K-band data. The continuum subtracted $H\alpha$ distribution (bottom left inset) is very different from either of the continuum maps. The $H\alpha$ emission comes from an elongated feature ($4'' \times 1.6''$) along p.a. 10 - 15° , approximately centred on J1c but peaking on either side of the continuum peak.

Figure 11 shows the near-IR spectra obtained with SPIFFI and integrated over the central J1 complex. As already found by Ivison et al. (2001), the rest-frame op-

tical/UV emission line spectrum is dominated by a starburst (HII region) spectrum without much evidence for AGN activity. The $H\alpha$ and [NII] line profiles exhibit blue wings with velocities of several hundred km/s and a [NII]/ $H\alpha$ line ratio of about 1 (indicated by the yellow line in the lower spectrum of Fig. 11).

These values are characteristic of shock-heated superwinds seen at low redshift. The J/H/K spectral energy distribution exhibits a break between the J and H bands that can be well fit by an A-star continuum model at redshift $z \sim 2.5$ (thick yellow line, age a few 10^2 Myrs). We interpret this emission as coming mainly from J1c and its extended surroundings (oval in Fig. 10), and conclude that J1c is a post-starburst stellar component at the same redshift as the young starburst and possibly part of the central bulge/disc of the submm source. The position of the powerful submm starburst, as marked by the mm CO line and continuum emission (Downes & Solomon 2003) is $\sim 0.5''$ ($\pm 0.4''$) NW of J1, somewhat offset from but still consistent with the location of the K-band peak. The $H\alpha$ line emission has a remarkably narrow profile (~ 130 km/s) and exhibits a systematic velocity gradient mainly in east-west direction, perpen-

dicular to its spatial elongation. J2 also shows $H\alpha$ emission, which is about 170 km/s offset from the systemic velocity of J1.

We can place the optical starburst features on the classical diagnostic diagrams. All diagnostic ratios ($[\text{OIII}]/H\beta$ vs $[\text{NII}]/H\alpha$, or $[\text{OI}]/H\alpha$ or $[\text{SII}]/H\alpha$) put the system firmly in the region of low excitation, low extinction ($E(B-V) \sim 0.4$) but high $H\alpha$ equivalent width, local starbursts. The density sensitive [SII] line ratio also indicates a very typical electron density of about 10^2 cm^{-3} . Perhaps most importantly we deduce a super-solar oxygen abundance ($12 + \log(\text{O}/\text{H}) \sim 9$) from the classical $(I([\text{OIII}]) + I([\text{OII}]))/I(H\beta)$ ratio. In addition, and somewhat surprisingly, the relatively strong [NII] emission relative to [OII] indicates that SMM 14011+0252 has relatively large nitrogen enrichment. These results are very significant since they pertain, in contrast to high-redshift QSO emission line regions, to large regions in the galaxy and imply that star formation has been proceeding in this system for a considerable period of time.

The morphology of the $H\alpha$ emission, its kinematics, the likely identification of J1c with a post-starburst component at the same redshift and the similar but not identical redshifts of J1 and J2 all can be explained in a simple lensing model where J1 and J2 are two physically associated background galaxies located behind the central cD of Abell 1835 that are magnified by about a factor of 4 to 6. The corresponding de-magnified images J1 (Fig.10 bottom insets) are fairly circular and point to a central dusty starburst (the submm source) surrounded by a low inclination and low extinction star forming disc ($H\alpha$ and optical continuum) of diameter about 8 kpc. The intrinsic luminosity

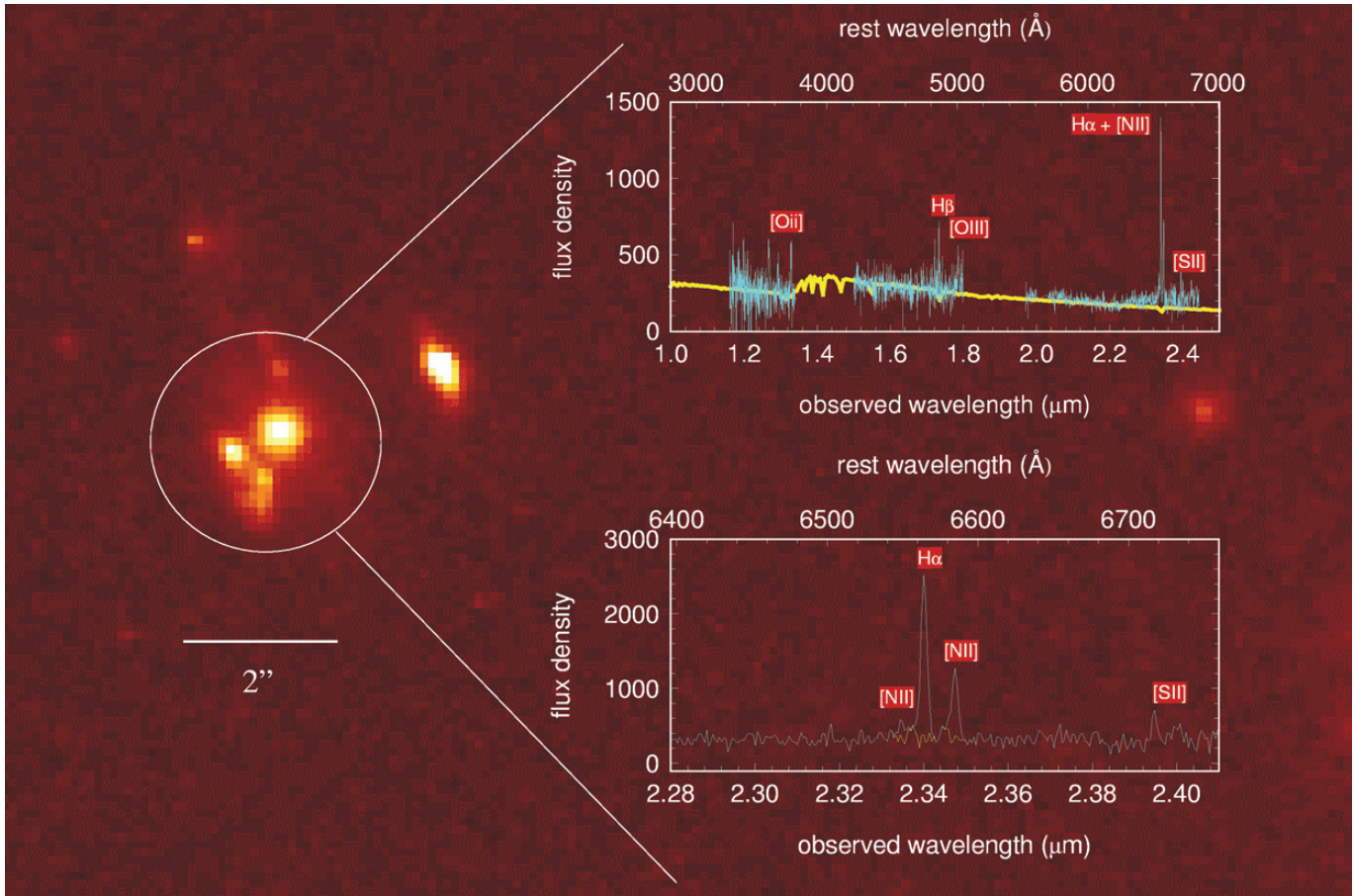


Figure 11: SPIFFI spectra of the central 2.5'' centred on J1c. The top right J/H/K spectrum shows a typical starburst emission line spectrum, plus a continuum with a spectral break between J and H that can be well fit by a few 10^2 Myr starburst (A-star spectrum) at redshift 2.5 (thick yellow curve). The bottom right zoom into the region around H α emission shows the narrow line widths, with a blueshifted residual wing that is probably due to a superwind (yellow curve).

of SMMJ14011+0252 then is about $4 \cdot 10^{12} L_{\odot}$, corresponding to a current star formation rate of ~ 300 to $700 M_{\odot}/\text{yr}$, depending on the IMF chosen. Assuming that this burst has been proceeding for the last 100 Myr – the minimum age derived from the continuum break – the inferred stellar mass formed in this burst is about $3\text{--}7 \cdot 10^{10} M_{\odot}$. For comparison the present (molecular) gas mass is about $2 \cdot 10^{10} M_{\odot}$ and the virial mass of the J1/J2 system is about $6 \cdot 10^{10} M_{\odot}$. While these numbers are obviously quite uncertain, they imply that SMMJ14011+0252 is a massive ($\sim m^*$) system forming in a major starburst event at $z \sim 2.5$, possibly triggered by the interaction of the J1/J2 components. Its luminosity is similar to those of very luminous local starbursts, such as the ULIRG mergers. Our conclusion is very much strengthened by the high metallicity of SMMJ14011+0252. The only low- z systems with such high a metallicity are massive ($\geq m^*$) early type galaxies. As our knowledge about the high- z submillimeter population increases, the evidence becomes firmer that these systems indeed must be precursors of massive local bulges and ellipticals.

This is in contrast to the Lyman break population whose evolutionary endpoint seems less clear.

OUTLOOK FOR SINFONI

SPIFFI is presently back in Europe for final tests and upgrades before mating with the ESO-delivered adaptive optics module for the full SINFONI instrument, which is based on MACAO, the Multiple Application Curvature Adaptive Optics toolbox (Bonnet et al. 2002). The present schedule foresees the acceptance tests of SINFONI early 2004. After shipment to Paranal, we expect first light at the telescope in April 2004. In addition to its seeing limited modes presented here, SINFONI will then be the world's first adaptive optics assisted near-IR integral field spectrometer. We hope that the instrument will be available to the general user community starting in fall 2004. In 2004, SPIFFI will also be retrofitted with a next generation $2K^2$ detector including its camera, presently under development by NOVA, ESO and MPE. Mating of SINFONI with the laser guide star facility (Bonaccini et al. 2003) is planned for spring 2005.

ACKNOWLEDGMENTS

The authors would like to thank H. Weisz, A. Goldbrunner, W.E. Zaglauer, and the MPE workshops and mechanical construction and electronics divisions, whose excellent work made the success of SPIFFI possible. We are also grateful to the ESO Garching and Paranal staff for their support, help and advice. We thank R. Ivison for giving us access to his R -band HST image of SMMJ14011+0252.

REFERENCES

- D. Bonaccini et al., 2003, *Proc. SPIE*, 4839, 381
- H. Bonnet et al., 2003, *Proc. SPIE*, 4839, 329
- D. Downes & P.M. Solomon, 2003, *ApJ*, 582, 37
- F. Eisenhauer et al., 2000, *Proc. SPIE*, 4008, 289
- F. Eisenhauer et al., 2003, *ApJ Letters* submitted (*astro-ph/0306220*)
- R. Genzel & C. J. Cesarsky, 2000, *ARAA*, 38, 761
- R. Genzel et al., 2003a, *ApJ* in press (*astro-ph/0305423*)
- R. Genzel et al., 2003b, *ApJ*, 584, 633
- A. Ghez et al., 2003, *ApJ*, 586, L127
- R. I. Ivison et al., 2001, *ApJ*, 561, L45
- S. Komossa et al., 2003, *ApJ*, 582, L15
- D. Lutz et al., 2003, *A&A*, in press (*astro-ph/0307552*)
- T. Ott et al., 2003, *ESO Messenger*, 111, 1
- M. J. Reid, 1993, *ARAA*, 31, 345
- M. Tecza et al., 2000, *ApJ*, 537, 178